# Quantum efficiency and metastable lifetime measurements in solid state laser materials via lock-in rate-window photothermal radiometry: technique and application to ruby ($Cr^{3+}:Al_2O_3$)

**Andreas Mandelis**
**Zhuo-Hui Chen**
**Ronald Bleiss***
University of Toronto
Department of Mechanical Engineering
Photothermal and Optoelectronic
Diagnostics Laboratory
Toronto, Canada, M5S 1A4

**Abstract.** The newly developed photothermal detection technique of rate-window infrared radiometry is applied to the measurement of the metastable state deexcitation parameters of a ruby laser rod. The technique employs a square laser pulse and monitors the infrared photothermal radiometric response of the sample. By applying the photothermal lock-in rate-window concept, the radiative lifetime and quantum efficiency of $Cr^{3+}:Al_2O_3$ are measured with optimal SNR and simple, unambiguous interpretation from the extremum in the lock-in analyzer in-phase rate-window signal. This technique simplifies significantly the experimental methodology; optimizes the photothermal SNR, which is inherently low in conventional frequency or time-domain photothermal measurements; and offers extended measurement dynamic range for both radiative quantum efficiency and lifetime in laser materials, as compared to frequency-scanned harmonic detection. Therefore, rate-window infrared photothermal radiometry may prove a valuable tool for the combined measurement of metastable lifetime and nonradiative energy conversion efficiency in laser materials with fast deexcitation rates.

*Subject terms: laser materials; rate-window photothermal detection; metastable lifetimes; radiometry; quantum efficiency.*

*Optical Engineering 32(9), 2046–2053 (September 1993).*

## 1 Introduction

Photoacoustic spectroscopy (PAS) was utilized early in the study of nonradiative processes in luminescent systems exhibiting metastable excited-state structure.[1,2] The advantage of this technique over purely optical methods is its ability to measure the absolute nonradiative quantum efficiency $\eta_{NR}$. This, in turn, can be readily used to determine the absolute radiative quantum efficiency $\eta_R = 1 - \eta_{NR}$ without recourse to complicated and often inaccurate absolute detector calibration procedures, such as the integrating sphere method, or knowledge of absolute ion concentrations in the case of solid state laser media.[3] This important feature of PAS was exploited by Murphy and Aamodt[4] in interpreting the observed concentration-dependent metastable level-quenching rates in ruby. Other authors have also applied PAS to the study of luminescence quantum efficiencies of laser-type solids[5,6] and liquids.[7] At the same time, the ability of PAS to yield measurements of metastable lifetimes in laser materials has been demonstrated, essentially independently from the quantum efficiency measurements.[1,8] These measurements were spectroscopic and, as a rule, difficult to interpret.

Quimby and Yen[9] have developed a working photoacoustic technique to determine $\eta_R$ in solid state laser materials, which depends on the measurement of the PAS phase. This technique can, in principle, estimate both the quantum efficiency $\eta_R$ and the metastable lifetime $\tau$. In addition to ruby, it has been used successfully with alexandrite.[10] In practice, however, there are several disadvantages: to eliminate the effects of both PAS saturation (i.e., the often nonlinear signal frequency response dependence on the optical absorption coefficient of the material), two optical excitation wavelengths are required with (ideally) equal absorption coefficients. This can be attained only if, by coincidence, the available laser source can operate at two separate lines at which the sample exhibits nearly equal absorption coefficients, as is the case of ruby and the krypton laser; the latter emits at 407 and 568 nm, for which lines the absorption coefficients $\beta$ are nearly equal in $E \perp c$ polarization[9] ($\beta \approx 41\ cm^{-1}$, $\Delta\beta = 1.2\ cm^{-1}$). A less accidental but more labor- and instrumentation-intensive method is to adjust the polarization of the laser beam by rotation with respect to the $c$ axis of the crystal[10] so that the absorptions at the two

*On leave from Jenoptik GmbH, Jena, Germany.

Invited paper OEC-13 received Jan. 29, 1993; revised manuscript received Mar. 16, 1993; accepted for publication Apr. 9, 1993.

operating lines become nearly equal. Under these nearly ideal conditions, and assuming one-dimensional PAS response, the PAS phase difference between the two signals at the two exciting wavelengths is a rather simple function of $\eta_{NR}$ and $\tau$, which yields these two parameters through the best fit of the theory to the data. This method, albeit very important as the simplest and most straightforward measurement technique of $\eta_{NR}$ (and consequently $\eta_R$) to date, unfortunately, does not guarantee the uniqueness of the two-parameter ($\eta_R$,$\tau$) fit. In addition, it is experimentally awkward and time consuming because it requires the aforementioned $\beta$ adjustment, coupled with two sets of frequency measurements, one at each excitation wavelength. Most importantly, (1) the required signal phase difference recording at each modulation frequency appears to produce significant scatter to the data, which compromises the measurement accuracy in an already low SNR situation, such as is the case with high-quality laser materials ($\eta_{NR}<0.1$), and (2) photoacoustic (PA) detection is intrinsically severely limited to low-frequency measurements by the significant roll-off of the microphone transfer function.[11] This important drawback limits the acceptable SNR to a range of lifetimes of several hundred microseconds, at best. Ruby [$\tau\approx 2.7$ ms (Ref. 9)] and alexandrite [$\tau = 260\mu$s (Ref. 10)] are only two of all the interesting and important laser materials with (usually) much shorter relaxation time constants. A case in point is the highly promising $Ti^{3+}$: $Al_2O_3$ crystal [$\tau\approx 3.3$ $\mu$s at $T = 300$ K (Ref. 12)]. It is necessary to be able to access modulation frequencies of the order of the inverse lifetime to obtain *both* $\eta_{NR}$ and $\tau$ information.

In a recent publication,[13] we sought to eliminate the deficiencies of the technique presented by Quimby and Yen.[9] For the first time, we demonstrated the suitability of infrared photothermal radiometry[14] (PTR) to the determination of $\eta_R$ and $\tau$ in a laser material (ruby). We further developed a simple analytical technique based on extrema in the PTR phase and amplitude slope, to obtain unambiguous $\eta_R$ and $\tau$ information from both amplitude and phase of the signal. We thus showed that these quantities can be determined self-consistently and uniquely from a single laser beam modulation frequency scan at one (arbitrary) excitation laser line, provided the photon energy can populate the metastable level. A severe problem associated with frequency-domain PTR of laser materials with short metastable level lifetimes (of the order of several microseconds, such as $Ti^{3+}$: sapphire rods) was subsequently discovered[15]: at the high modulation frequencies (greater than 100 kHz) required to access the rates of delayed heating of these materials following nonradiative decay of the excited metastable level(s), the PTR signal magnitudes are very low because of the $f^{-1}$ dependence of the lock-in amplifier-measured amplitude predicted for nonopaque $Al_2O_3$-based solid state laser materials[13,16] and observed in our experiments.[13] As a result, the expected extrema in the PTR amplitude and phase occur in the neighborhood of $f = 100$ kHz for $Ti^{3+}$: $Al_2O_3$ (Ref. 15) with an SNR too low to derive meaningful values of the desired parameters ($\eta_R$ and $\tau$).

In this paper, the infrared photothermal rate-window methodology recently developed in our laboratory[17] is applied for the first time to the study of the metastable state decay kinetics of a ruby rod and is shown to be a very promising alternative to the frequency-domain PTR as a viable candidate for the study of other laser materials with short metastable level lifetimes.

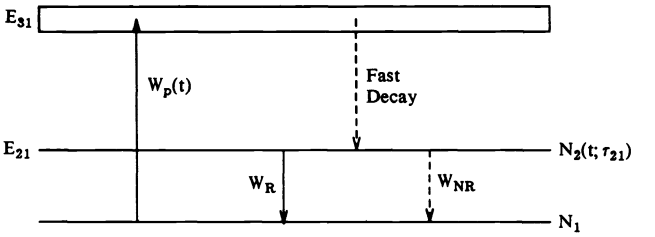


**Fig. 1** Simplified electronic energy kinetics diagram from a three-level system, such as ruby ($Cr^{3+}$: $Al_2O_3$).

## 2 Time-Resolved PTR of Laser Materials

For a solid state laser medium exhibiting three-level dynamic behavior, such as $Cr^{3+}$: $Al_2O_3$, Fig. 1, under the time-gated square-pulse excitation of a rate-window type of experiment,[17] the rate equation for level $|2\rangle$ is given by

$$\frac{d}{dt}N_2(t) = N_1 W_p(t) - \frac{N_2(t)}{\tau_{21}} , \tag{1}$$

where

$$\tau_{21} = \frac{1}{W_R + W_{NR}} , \tag{2}$$

with $W_R$ and $W_{NR}$ being the probabilities for radiative and nonradiative decay, respectively. In Eq. (1) it is assumed that $N_1$ is constant,[9] a condition valid for sufficiently weak pumping of the ground state $|1\rangle$, which is also always heavily populated in a three-level laser medium. The pumping rate $W_p(t)$ to level $|3\rangle$ is given by

$$W_p(t) = \begin{cases} W_{p0} , & t<\tau_p \\ 0 , & t>\tau_p \end{cases} , \tag{3}$$

where $\tau_p$ is the square laser pulse duration. The solution to rate Eq. (1) under the initial condition $N_2(t=0) = 0$ is

$$N_2(t;\tau_{21}) =$$

$$N_1 W_{p0} \tau_{21} \begin{cases} 1 - \exp(-t/\tau_{21}) , & t \leq \tau_p \\ [\exp(\tau_p/\tau_{21}) - 1]\ \exp(-t/\tau_{21}) , & t \geq \tau_p \end{cases} . \tag{4}$$

As the result of the nonradiative decays in the optical medium, which include the relatively slow $|2\rangle \rightarrow |1\rangle$ decay preceded by the fast nonradiative $|3\rangle \rightarrow |2\rangle$ transition, the thermal power density in J/cm$^3$s released in the laser material is

$$A(t) = N_1 E_{32} W_p(t) + \left(\frac{\eta_{NR}}{\tau_{21}}\right) E_{21} N_2(t;\tau_{21}) , \tag{5}$$

where

$$\eta_{NR} = 1 - \eta_R = \frac{\tau_{21}}{\tau_{NR}} = \frac{W_{NR}}{W_R + W_{NR}} . \tag{6}$$

The increase in the surface temperature of the laser medium can be monitored using infrared photothermal radiometric

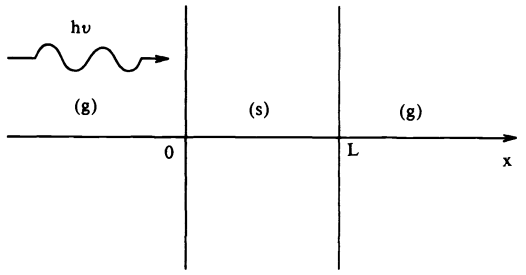


**Fig. 2** Schematic of one-dimensional geometry for back-scattered infrared photothermal radiometry of a three-level solid-state laser material; (*g*): gas (air) layer and (*s*): solid layer of thickness $L$ and optical absorption coefficient $\beta_{31}(\lambda)$.

detection. For this purpose, three coupled heat diffusion equations can be set up corresponding to the experimental geometry of Fig. 2:

$$\frac{1}{\alpha_g}\frac{\partial T_g(x,t)}{\partial t}-\frac{\partial^2 T_g(x,t)}{\partial x^2}=0\,,\quad x\leq 0 \text{ and } x\geq L\,, \tag{7a}$$

$$\frac{1}{\alpha_s}\frac{\partial T_s(x,t)}{\partial t}-\frac{\partial^2 T_s(x,t)}{\partial x^2}=\frac{A(t)}{k_s}\exp(-\beta_{31}x)\,,\quad 0\leq x\leq L\,, \tag{7b}$$

where $\alpha_j$ is the thermal diffusivity of the $j$'th layer, $k_s$ is the solid thermal conductivity, and $\beta_{31}(\lambda)$ is the absorption coefficient of the optical medium ($s$) at the excitation wavelength and is proportional to the population of level $|1\rangle$:

$$\beta_{31}(\lambda)=N_1(W_{p0}E_{31}/I_0)\,, \tag{8}$$

where $I_0$ in watts per centimeters squared is the incident laser intensity. Equations (7a) and (7b) can be Laplace transformed[18] using

$$\hat{A}(s)=\int_0^\infty e^{-st}A(t)\,dt=I_0\beta_{31}R[1-\exp(-s\tau_p)]\times\left[\frac{1}{s}+Q\left(\frac{1}{s}-\frac{1}{s+\tau_{21}^{-1}}\right)\right]\,, \tag{9}$$

where Eqs. (3) to (5) were used along with

$$R\equiv E_{32}/E_{31}\,, \tag{10a}$$

and

$$Q\equiv\eta_{NR}(E_{21}/E_{32})\,. \tag{10b}$$

Temperature and heat flux continuity at the solid-gas interfaces[18] yield the Laplace transform of the solid surface temperature

$$\hat{T}_s(x=0;s)=\frac{\hat{A}(s)\exp(-a_sL)}{k_s(\beta_{31}^2-a_s^2)[1-\exp(-2a_sL)]}[(r_{31}-1)\exp(a_sL)+(r_{31}+1)\exp(-a_sL)-2r_{31}\exp(-\beta_{31}L)]\,, \tag{11}$$

where

$$a_s(s)\equiv(s/\alpha_s)^{1/2}\,,\quad r_{31}(s)\equiv\frac{\beta_{31}}{a_s(s)}\,. \tag{12}$$

For PTR detection at early times following the optical pulse, such that $t<<\tau_L\equiv(\alpha_sL^2)^{-1}$, the material is thermally semi-infinite, i.e.,

$$\exp(-a_sL)\simeq 0\,. \tag{13}$$

Under this condition, Eq. (11) becomes

$$\hat{T}_s(x=0;s)=\frac{I_0\beta_{31}\alpha_sR\tau_\beta^{1/2}}{k_s}[1-\exp(-s\tau_p)]\times\left\{(1+Q)\left[\frac{1}{s^{3/2}}-\frac{1}{s(s^{1/2}+\tau_\beta^{-1/2})}\right]-Q\left[\frac{1}{s^{1/2}(s+\tau_{21}^{-1})}-\frac{1}{(s^{1/2}+\tau_\beta^{-1/2})(s+\tau_{21}^{-1})}\right]\right\}\,, \tag{14}$$

where

$$\tau_\beta\equiv(\beta_{31}^2\alpha_s)^{-1} \tag{15}$$

is a thermal transit time from a depth in the absorbing solid equal to the optical absorption length[19] $1/\beta_{31}$. Table 1 shows inverse Laplace transforms useful in obtaining the transient thermal pulse description $T_s(0;t)$. For the particular case of a ruby crystal, it was found that $\beta_{31}(514.5\text{ nm})=0.325\text{ cm}^{-1}$ at the 514.5-nm line of the $Ar^+$ laser.[13] Furthermore, using the value of thermal diffusivity $\alpha_s=0.13\text{ cm}^2/s$ (Ref. 20) in Eq. (15) yields $\tau_\beta\simeq 72.8\ s\gg s^{-1}\leftrightarrow t$, i.e., $\tau_\beta^{-1/2}$ can be set equal to zero in Eq. (14) for the observation times of experimental interest in this work ($t\leq 5$ ms). As a result of this approximation, Eq. (14) becomes simplified as follows:

$$\hat{T}_s(0;s)\simeq I_0\left(\frac{\beta_{31}\alpha_s}{k_s}\right)R[1-\exp(-s\tau_p)]\times\left[\frac{1+Q}{s^2}-\frac{Q}{s(s+\tau_{21}^{-1})}\right]\,. \tag{16}$$

The time-resolved PTR back-scattered signal is proportional to the inverse Laplace transform[18,21] of Eq. (16):

$$S_B(t)=C\tau_{21}\times\begin{cases}(1+Q)(t/\tau_{21})-Q[1-\exp(-t/\tau_{21})], & t\leq\tau_p\\ (1+Q)(\tau_p/\tau_{21})-Q[\exp(\tau_p/\tau_{21})-1]\exp(-t/\tau_{21}), & t\geq\tau_p\end{cases}\,, \tag{17}$$

where

$$C=\text{const.}\times(I_0R\beta_{31}\alpha_s/k_s)\,. \tag{18}$$

**Table 1** Laplace transform pairs necessary for the inversion of Eq. (14).

| $f(s) = \int_o^\infty e^{-st} F(t)dt$ | $F(t)$ |
|---|---|
| $\frac{1}{s^{3/2}}$ | $2\sqrt{t/\pi}$ |
| $\frac{1}{s(s^{1/2} + \tau_\beta^{-1/2})}$ | $\tau_\beta^{1/2}\left(1 - e^{t/\tau_\beta}\,\mathrm{erfc}\sqrt{t/\tau_\beta}\right)$ |
| $\frac{1}{s^{1/2}(s + \tau_{21}^{-1})}$ | $2\sqrt{\frac{\tau_{21}}{\pi}}\,e^{-t/\tau_{21}}\,G(\sqrt{t/\tau_{21}})$ |
| $\frac{1}{(s^{1/2} + \tau_\beta^{-1/2})(s + \tau_{21}^{-1})}$ | $2\sqrt{\frac{\tau_{21}}{\pi}}\left(1 - \frac{T}{\tau_\beta}\right)e^{-t/\tau_{21}}\,G(\sqrt{t/\tau_{21}}) - \frac{T}{\tau_\beta^{1/2}}\left(e^{t/\tau_\beta}\,\mathrm{erfc}\sqrt{t/\tau_\beta} - e^{-t/\tau_{21}}\right)$ |

Definitions:

$$\mathrm{erfc}(x) \equiv \frac{2}{\sqrt{\pi}}\int_x^\infty e^{-y^2}dy$$

$$G(x) \equiv \int_o^x e^{y^2}dy$$

$$T \equiv (\tau_\beta^{-1} + \tau_{21}^{-1})^{-1}$$

Computer simulations of the exact inverse of $\hat{T}_s(0;s)$, Eq. (14) (see Table 1), and of the approximate Eq. (17) showed identical time evolution at early times with significant deviations for $t>50$ ms.

## 3 Scanning Photothermal Rate-Window PTR

In terms of physical information content, frequency-domain and time-domain photothermal methodologies are completely equivalent, in principle. In terms of signal interpretation, the latter technique is considered preferable because of the inherent ability of transient-response methods to be interpretable by simple system time-delay constants. Furthermore, the Fourier transform pair relationship existing between time and frequency domains renders impulse-response photothermal signals (such as those PTR signals produced by a pulsed laser) vastly advantageous in monitoring fast events, i.e., with time constants commensurate with the early decay of the system photothermal response, when signals are strongest. On the other hand, owing to the small energy content, the frequency-domain photothermal response is weakest (accompanied by the lowest SNR) at the highest frequencies, which must be utilized to adequately probe events causing delays in thermal energy release.[13]

Despite the enormous SNR advantage of pulsed-laser photothermal methods, when nonradiative energy release delays from highly efficient optical materials must be measured, the coefficient $Q$, Eq. (10b), is usually very low (e.g., it is approximately 10% for ruby, because $\eta_{NR} \lesssim 5\%$ in that material[9] and $E_{21}/E_{32} = 2.88$ for 514.5-nm $Ar^+$-ion laser excitation). Therefore, small shifts in signal baseline or even the normal variance in the value of the photothermal transients instrumentally averaged to achieve an acceptable SNR, may totally invalidate or grossly distort the value of $Q$ thus measured.

In the case of pulsed PTR, the most serious disadvantage of wideband pulsed detection of laser materials using conventional HgCdTe (MCT) detectors is the baseline drift inevitably introduced from shot to shot in the measurement as a result of the passage of the dc level through the associated preamplifier. To overcome the dc background thermal radiation limitation and improve the time-resolved PTR measurement SNR in the more forgiving case of nonoptical solids, Cho and Davis[22] normalized their photothermal transients (256 shots) by subtracting 256 shots of the detector dc background after blocking the incident laser beam.

In this paper, we introduced the recently developed[17] technique of lock-in rate-window PTR to perform accurate measurements of $Q$ (and, therefore, of $\eta_{NR}$) in ruby. The lock-in rate-window method has the distinct advantage of combining the superior SNR of a tuned electronic filter (familiar with frequency domain PTR detection, which efficiently eliminates the dc level) needed for a sensitive measurement of very low optical-to-thermal energy conversion coefficients $Q$, with the superior signal strength, characteristic of the early-time PTR response to a pulsed (actually, intensity "time-gated" cw) laser.

This optimized signal circumstance can be easily achieved by acousto-optically generating a repetitive, time-gated, laser pulse and introducing the (also repetitive) time-resolved PTR response of the laser material to a lock-in analyzer operating

at the pulse repetition reference frequency $f_0$, with a long filter time constant. In this instrumental mode, we measured the in-phase (IP) signal resulting from the lock-in analyzer, which amounts to the fundamental Fourier component $b_1$ of the back-scattered PTR signal, $S_B(t)$, over the pulse repetition period $T_0$ (Ref. 23):

$$b_1(\tau;T_0)=\frac{2}{T_0}\int_0^{T_0} S_B(t;\tau)\ \sin(\omega_0 t)\ dt\ , \tag{19}$$

where $\tau$ is a physical time constant of the probed system, such as $\tau_{21}$, and

$$\omega_0\equiv\frac{2\pi}{T_0}=2\pi f_0\ . \tag{20}$$

Equation (19) exhibits a maximum if the repetition period $T_0$ of the laser pulse is varied. The IP component of the lock-in output can be shown to be given by[23]

$$S_{IP}(\tau;T_0)=\frac{2}{\pi}b_1(\tau;T_0)\ , \tag{21}$$

so that the condition for the existence of an extremum becomes

$$\frac{\partial}{\partial T_0}b_1(\tau;T_0)=0\ . \tag{22}$$

The details of extracting $\tau$-related information from the (usually nonalgebraic) Eq. (22) depend on the functional dependence of $S_B(t)$ on this parameter. In this work we used luminescence lock-in rate-window signals from a ruby sample to measure $\tau_{21}$ optically from Eq. (4), with the photodiode signal being proportional to $N_2(t;\tau_{21})$. PTR rate-window signal analysis was based on Eq. (17).

## 4 Experiment and Discussion

Experiments were performed to obtain both the photothermal (PTR) and luminescence lock-in rate-window response of a cylindrical ruby sample, 6 cm in length and 1 cm in diameter.[13] The two flat surfaces were polished smooth, whereas the curved surface was rough and light scattering. The $Cr^{3+}$ concentration of the sample was unknown. Quimby and Yen[9] have remarked that the potential existence of trap levels 100 to 200 $cm^{-1}$ below the single-ion $^2E$ level, which appear in the fluorescence spectra of ruby crystals of moderate to high $Cr^{3+}$ concentrations ($\lesssim$0.4 at. %), may invalidate the three-level diagram of Fig. 1 at low temperatures. Such traps become relaxation rate limiting with shorter lifetimes than that of the single-ion levels. Nevertheless, at room temperature, the traps and single-ion levels are in thermal equilibrium, and thus can be adequately represented by one level with a single lifetime, irregardless of the actual $Cr^{3+}$ concentration. Figure 3 shows the dual experimental setup: A cw Innova 100 $Ar^+$ laser from Coherent was used as an unfocused pump of spot size approximately 1 mm and with output power less than or equal to 2.5 W at 514.5 nm. The blackbody radiation from the optically excited ruby crystal surface was collected and collimated by two Ag-coated off-axis paraboloidal mirrors,

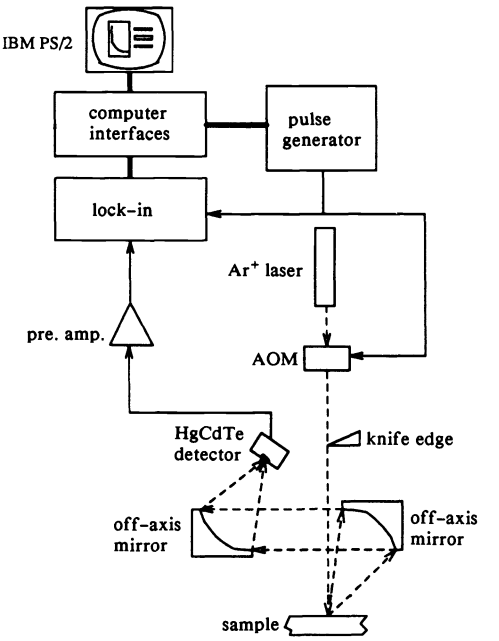


**Fig. 3** Experimental setup for PTR and luminescence lock-in rate-window measurements; AOM: Acousto-optic modulator, HgCdTe detector: EG & G Judson Model J15-D12, dc-coupled with fitted Ge window.

and subsequently focused on the active area of a HgCdTe detector (EG & G Judson Model J15D12)/preamplifier element with frequency bandwidth between dc and 1 MHz. The detector was fitted with a Ge window, which filtered out the excitation beam. The spectral response bandwidth of the detector was in the 8- to 12-$\mu$m range. The PTR signal from the preamplifier (EG & G Judson Model PA-350) was fed into an EG & G Model 5210 lock-in analyzer. An external reference pulsed voltage generator of duration $\tau_p$ and repetition period $T_0$ was used to drive the acousto-optic modulator (AOM) and to automatically change the modulation frequency (period) applied to it. This setup therefore allowed computer-controlled, automatic-repetition-period scans of the time-gated laser intensity. Luminescence emitted through the curved side surface of the optically pumped ruby rod was filtered from excitation line photons using a sharp cutoff glass filter (Melles-Griot Model 0G550) acting as a low-pass filter in front of a fast (nanosecond) risetime Si photodiode. The photovoltage generated by the spectrally integrated luminescence of our crystal, the spectrum of which is shown in Fig. 4, was fed into an EG & G Model 5210 lock-in analyzer and the amplitudes and phases of both PTR and luminescence signals were stored in the computer. The linearity of luminescence signals with excitation intensity was ascertained in preliminary experimental runs using conventional harmonic lock-in detection. The validity of the three-level theoretical description leading to Eq. (4) was further tested by monitoring the actual time evolution of the time-gated luminescence signals and verifying agreement with that equation, as indicated by purely exponential buildup ($t<\tau_p$) and exponential decay ($t>\tau_p$) of the signal on a transient Tektronix oscilloscope. Further general agreement of the time-gated PTR signals with Eq. (17) was observed with a superposed baseline drift, as discussed earlier.

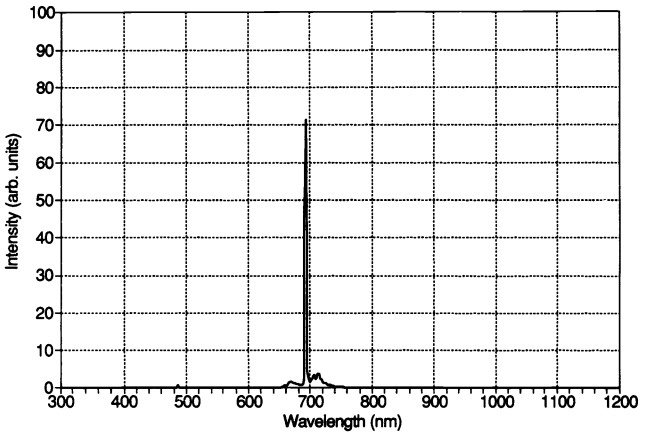


**Fig. 4** Ruby crystal luminescence spectrum. Note the strong domination of the $^2E$ metastable state luminescence at 694.5 nm.

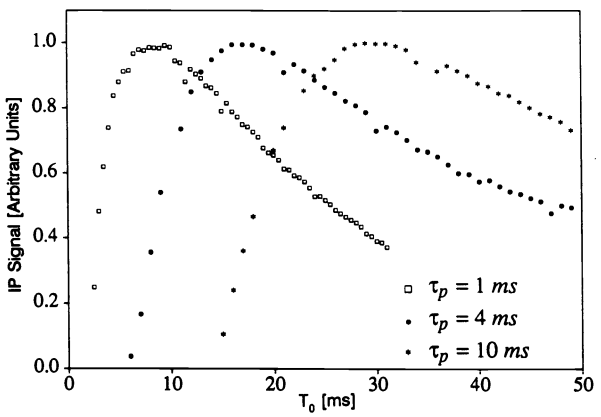


**Fig. 5** In-phase lock-in rate-window luminescence signals from a ruby crystal. Pulse duration $\tau_p$: (□) 1 ms, (·) 4 ms, and (*) 10 ms.

Figure 5 shows the IP luminescence rate-window signals for three pulse durations $\tau_p$: 1, 4, and 10 ms. The lock-in signal extremum was analyzed using Eq. (4) in the integrand of Eq. (19). The result of the integration is ($\tau_p \leq T_0$):

$$b_1(\tau_{21};T_0)=C\tau_{21}\left[1-\cos(\omega_0\tau_p)+\frac{\omega_0}{(\tau_{21}^{-2}+\omega_0^2)^{1/2}}\right.$$
$$\times\left(\sin(\omega_0\tau_p+\theta)-\{1+\exp[-(T_0-\tau_p)/\tau_{21}]\right.$$
$$\left.\left.-\exp(-T_0/\tau_{21})\}\sin\theta\right)\right] , \quad (23)$$

where

$$\theta=\tan^{-1}(\omega_0\tau_{21}) . \quad (24)$$

In this case, the condition for the extremum, Eq. (22) with $\tau=\tau_{21}$, yields the simple linear relationship

$$(T_0)_{\max}=2.5681\tau_{21}+1.9973\tau_p . \quad (25)$$

The range of $\tau_{21}$ values obtained from all three curves in Fig. 5 was

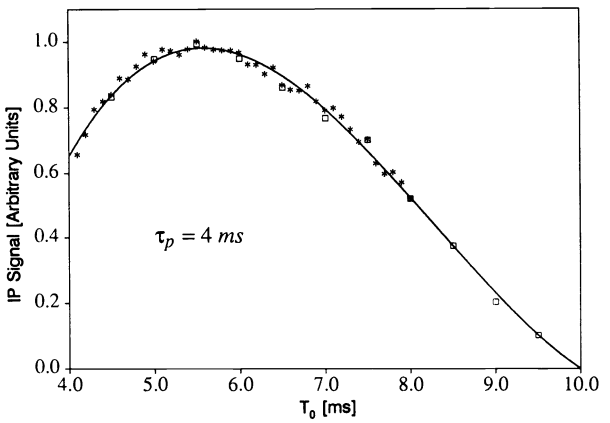


**Fig. 6** In-phase lock-in rate-window PTR signals from the ruby crystal. Pulse duration $\tau_p=4$ ms. Data points from two independent scans (***;□□□) are superposed on a polynomial fit (−) to Eq. (27). The maximum occurs at $T_0=5.5$ ms.

$$\tau_{21}=3.789\pm0.14 \text{ ms} , \quad (26)$$

in excellent agreement with our earlier calculations[13] using frequency-domain PTR. Note that the variance in the value of $\tau_{21}$, obtained by both (harmonic modulation and rate-window) luminescence methods was found to be comparable, as expected by the high dynamic range of optical signals. In this case, there is no apparent advantage of the rate-window method.

The results of the rate-window PTR measurements on ruby are shown in Fig. 6. The data points on this figure belong to two separate experimental runs and their low scatter is a measure of the excellent reproducibility of this technique. The lock-in IP signal maximum was analyzed using Eq. (17) in the integrand of Eq. (19), again with $\tau=\tau_{21}$. The result of the integration, written in a form that highlights the dependence on the quantity of interest $Q$ (provided $\tau_p \leq T_0$) is

$$b_1(\tau_{21},Q;T_0)=(1+Q)b_{11}(\tau_{21};t_0)-Qb_{12}(\tau_{21};T_0) , \quad (27)$$

where

$$b_{11}(\tau_{21};T_0)=\frac{1}{\pi\tau_{21}}[\omega_0^{-1}\sin(\omega_0\tau_p)-\tau_p] , \quad (28a)$$

and

$$b_{12}(\tau_{21};T_0)=\frac{1}{\pi}\left[[1-\cos(\omega_0\tau_p)]+\frac{\omega_0\tau_{21}}{[1+(\omega_0\tau_{21})^2]^{1/2}}\right.$$
$$\times\left(\sin(\omega_0\tau_p+\theta)-\{1+\exp[-(T_0-\tau_p)/\tau_{21}]\right.$$
$$\left.\left.-\exp(-T_0/\tau_{21})\}\sin\theta\right)\right] . \quad (28b)$$

The value for $\tau_{21}$ entered in the theoretical simulations of Eqs. (27) and (28) was the one determined experimentally from the luminescence measurement, Eq. (26). Figure 7 shows that for the range of $\tau_{21}$ values obtained experimen-

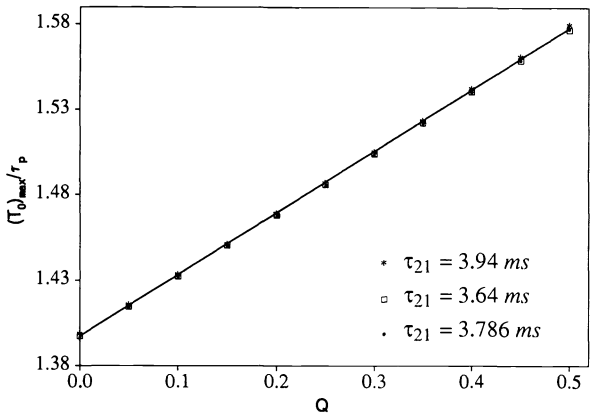


**Fig. 7** Simple dependence of the lock-in rate-window maximum on the optical-to-thermal energy conversion efficiency $Q$ of ruby: (***)$\tau_{21}=3.94$ ms, (···)$\tau_{21}=3.78$ ms, (□□□)$\tau_{21}=3.64$ ms, and pulse duration $\tau_p=6$ ms. The straight line is there to aid the eye.

tally, the condition for the rate-window extremum, Eq. (22) with $b_1(\tau_{21},Q;T_0)$ from Eq. (27), yields a simple, nearly linear dependence on $Q$. In the range of experimentally expected $Q$ values (less than 50%) with $\tau_p=6$ ms, the relationship shown in Fig. 7 can be expressed numerically as

$$(T_0)_{max}/\tau_p=0.361\ Q+1.397\ . \tag{29}$$

The linearity of the $(T_0)_{max}/\tau_p$ versus $Q$ relation improves with increased $\tau_p$. For this reason, Eq. (29) was shown to predict $Q$ values consistent with those obtained with other values $\tau_p>2$ ms, and therefore was used for subsequent calculations. The large slope of, together with the small variance in, the data of Fig. 7 demonstrate the high sensitivity of lock-in rate-window PTR to the value of $Q$. The IP signal curve (polynomial fit) equivalent to Fig. 6 for $\tau_p=6$ ms exhibited its maximum at $(T_0)_{max}=8.65$ ms, i.e., for $(T_0)_{max}/\tau_p=1.44$. From Fig. 7, one thus obtains $Q=0.121$. Using[13] $E_{21}=1.79$ eV and $E_{32}=0.62$ eV in the $Q$-defining Eq. (10b), one obtains the value of nonradiative quantum efficiency:

$$\eta_{NR}=0.042\pm0.006\ . \tag{30}$$

This new value is in excellent agreement with $\eta_{NR}=0.04$, the value calculated using the harmonically modulated PTR phase in Ref. 13. It is, however, at the low limit of the range of values calculated indirectly by Quimby and Yen.[9] Those authors found $\eta_R=0.90\pm0.05$, which implies $\eta_{NR}=0.10\pm0.05$. Note the greater standard deviation value reported by Quimby and Yen, most likely the result of using conventional frequency-domain phase data with lower thermal contents in the frequency range 10 to 1000 Hz than the early portions of the time-gated pulses used in rate-window PTR. Shand[10] reported a standard deviation in PAS phase data similar to Quimby and Yen's for alexandrite. The standard deviation reported in Eq. (30) was obtained by using rate-window data from consecutive experimental runs. The SNR of the rate window IP signal, Fig. 6, is superior to that of the PTR phase,[13] as expected from theory,[17] which makes the present value of $\eta_{NR}$ more reliable. This advantage in SNR of rate-window PTR becomes more pronounced with shorter $\tau_{21}$, for which the required probe modulation frequency range has very low thermal energy content. Our preliminary rate-window and frequency-domain PTR measurements on $Ti^{3+}$: $Al_2O_3$ crystals[24] ($\tau_{21}\simeq3.8$ μs), have generated stable IP signals (rate-window), but unfortunately, the phase signal extremum (frequency-domain) occurs at approximately 100 kHz with standard deviation approximately 1 deg, which exceeds the shift expected due to the delayed heat release (less than 0.5 deg). These results will be reported in a future publication.

## 5 Conclusions

Self-consistent PTR and luminescence scanned rate-window measurements of a ruby laser rod were performed. The data were analyzed in terms of photothermal and optical time-resolved models, respectively, of a conventional three-level solid-state laser medium. Expressions were found for the extremum in the in-phase (IP) response curve of the PTR signal as well as for the extremum in the luminescence rate-window signal. In practice, the optimal combination of measurements in terms of SNR for solid state laser material parameters involves the luminescence extremum ($\tau_{21}$) and the PTR maximum ($Q\rightarrow\eta_{NR}\rightarrow\eta_R=1-\eta_{NR}$). The superior SNR and dynamic range of rate-window PTR is, in principle, capable of extending these measurements to solid state lasers with submillisecond lifetimes and work is in progress on the $Ti^{3+}$: $Al_2O_3$ system.

The present work has demonstrated that the high-frequency/small-signal limitations of frequency-domain PTR, real impediments to any noncontact, reliable photothermal measurement of $\eta_{NR}$ in solid state lasers,[9,10] can be efficiently overcome using IP rate-window detection. The latter combines the superior dynamic reserve of the lock-in analyzer with long filter time constant, with the considerable thermal energy content/signal strength of the early time transient photothermal response to an exciting laser pulse.

### Acknowledgments

The authors gratefully acknowledge a strategic grant from the Natural Sciences and Engineering Research Council of Canada (NSERC), which made this work possible.

### References

1. L. D. Merkle and R. C. Powell, "Photoacoustic spectroscopy investigation of radiationless transitions in $Eu^{3+}$ ions in KCl crystals," *Chem. Phys. Lett.* **46,** 303–306 (1977).
2. A. Rosencwaig and E. A. Hildum, "$Nd^{3+}$ fluorescence quantum-efficiency measurements with photoacoustics," *Phys. Rev. B* **23,** 3301–3307 (1981).
3. R. S. Quimby and W. M. Yen, "Photoacoustic measurement of absolute quantum efficiencies in solids," *Opt. Lett.* **3,** 181–183 (1978).
4. J. C. Murphy and L. C. Aamodt, "Photoacoustic spectroscopy of luminescent solids: ruby," *J. Appl. Phys.* **48,** 3502–3509 (1977).
5. J. Hamilton, I. Duncan, and T. Morrow, "Anomalous wavelength-dependent effects in photoacoustic measurements of $Nd^{3+}$ luminescence quantum efficiency in various laser materials," *J. Lumin.* **33,** 1–33 (1985).
6. A. Mandelis, "Photoacoustic determination of the non-radiative quantum efficiency of uranyl formate monohydrate, $UO_2(HCOO)_2{\cdot}H_2O$, powders," *Chem. Phys. Lett.* **91,** 501–505 (1982).
7. W. Lahmann and H. J. Ludewig, "Opto-acoustic determination of absolute quantum yields in fluorescent solution," *Chem. Phys. Lett.* **45,** 177–179 (1977).
8. R. C. Powell, D. P. Neikirk, J. M. Flaherty, and J. G. Gualtieri, "Lifetime measurements, infrared and photoacoustic spectroscopy of $NdP_5O_{14}$," *J. Phys. Chem. Solids* **41,** 345–350 (1980).
9. R. S. Quimby and W. M. Yen, "Photoacoustic measurement of the ruby quantum efficiency," *J. Appl. Phys.* **51,** 1780–1782 (1980).

10. M. L. Shand, "Quantum efficiency of alexandrite," *J. Appl. Phys.* **54,** 2602–2604 (1983).
11. A. Mandelis and B. S. H. Royce, "Relaxation time measurements in frequency and time-domain photoacoustic spectroscopy of condensed phases," *J. Opt. Soc. Am.* **70,** 474–480 (1980).
12. P. Albers, E. Stark, and G. Huber, "Continuous-wave laser operation and quantum efficiency of titanium-doped sapphire," *J. Opt. Soc. Am. B.* **3,** 134–139 (1986).
13. A. Mandelis, M. Munidasa, and A. Othonos, "Single-ended infrared photothermal radiometric measurement of quantum efficiency and metastable lifetime in solid-state laser materials: the case of ruby ($Cr^{3+}$:$Al_2O_3$)," *IEEE J. Quantum Electron.* (in press).
14. A. C. Tam, "Pulsed laser photoacoustic and photothermal detection," in *Photoacoustic and Thermal-Wave Phenomena in Semiconductors,* A. Mandelis, Ed., pp. 176–197, North-Holland, New York (1987).
15. M. Munidasa and A. Mandelis, Unpublished (1992).
16. R. D. Tom, E. P. O'Hara, and D. Benin, "A generalized model of photothermal radiometry," *J. Appl. Phys.* **53,** 5392–5400 (1982).
17. Z. Chen and A. Mandelis, "Thermal-diffusivity measurements of ultrahigh thermal conductors with use of scanning photothermal rate-window spectrometry: chemical-vapor-deposition diamonds," *Phys. Rev. B* **46,** 13526–13538 (1992).
18. R. Santos and L. C. M. Miranda, "Theory of the photothermal radiometry with solids," *J. Appl. Phys.* **52,** 4194–4198 (1981).
19. A. Mandelis and B. S. H. Royce, "Time-domain photoacoustic spectroscopy of solids," *J. Appl. Phys.* **50,** 4330–4338 (1979).
20. W. Koechner, *Solid State Laser Engineering,* Springer Series in Optical Sciences, Vol. 1, Chap. 2.2, pp. 44–53, New York (1976).
21. W. P. Leung and A. C. Tam, "Techniques of flash radiometry," *J. Appl. Phys.* **56,** 153–161 (1984).
22. K. Cho and C. C. Davis, "Time-resolved infrared radiometry of laser-heated silicon," *IEEE J. Quantum Electron.* **25,** 1112–1117 (1982).
23. A. Mandelis and Z. Chen, "Lock-in rate-window thermomodulation (thermal wave) and photomodulation spectrometry," *Rev. Sci. Instrum.* **63,** 2977–2988 (1992).
24. Z. Chen, M. Munidasa, and A. Mandelis, Unpublished (1992).

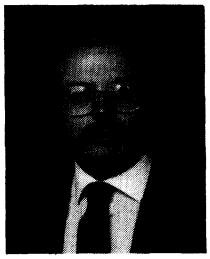

**Andreas Mandelis** received the BSc degree in physics, magna cum laude, in 1974 from Yale University. He received the MA degree in applied physics in 1976, the MSE degree in mechanical and aerospace engineering in 1977, and the PhD in applied physics in 1979 from Princeton University, New Jersey. He was a member of the scientific staff (silicon R&D) at Bell Northern Research, Ottawa, Ontario, from 1980 to 1981, an assistant professor in the Department of Mechanical Engineering at the University of Toronto from 1982 to 1986; an associate professor from 1986 to 1990, and is currently a full professor and director of the Photothermal and Optoelectronic Diagnostics Laboratory. His major interests are the development of new photothermal devices, the science and technology of photothermal detection and its application to optoelectronic materials, instrumentation and measurement, and materials research. Dr. Mandelis is a member of the American Physical Society, Sigma Xi, Canadian Association of Physicists, Applied Spectroscopy, IEEE, and ASME.

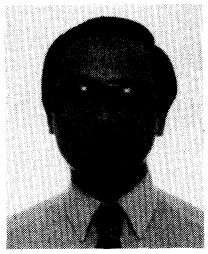

**Zhuo-Hui Chen** received his undergraduate degree in 1982 from Huazhong University of Science and Technology, Wuhan, China. He received the PhD degree in 1989 from Tohoku University, Research Institute of Electrical Communication, Sendai, Japan. He was a research associate with the Photothermal and Optoelectronic Diagnostics Laboratory, University of Toronto, from 1989 until 1993. He is currently with Northern Telecom in Ottawa, Canada.

**Ronald Bleiss** completed a 5-year Master of Physics degree at Humbolt University of Berlin in 1989. His professional career began the same year with the firm Carl-Zeiss Jena GmbH as research assistant and he is still with the same company, renamed CZJ, Jenoptik GmbH. He is currently on leave at the University of Toronto, Photothermal and Optoelectronic Diagnostics Laboratory, Department of Mechanical Engineering, on a German Government-assisted work program.